American Mineralogist, Volume 90, pages 1500–1505, 2005

Effects of high pressure and high temperature on cation ordering in magnesioferrite, $MgFe_2O_4$, using in situ synchrotron X-ray powder diffraction up to 1430 K and 6 GPa

SYTLE M. ANTAO,[1,*] ISHMAEL HASSAN,[2] WILSON A. CRICHTON,[3] AND JOHN B. PARISE[1]

[1]Mineral Physics Institute and Department of Geosciences, State University of New York, Stony Brook, New York 11794-2100, U.S.A.
[2]Department of Chemistry, University of the West Indies, Mona, Kingston 7, Jamaica
[3]European Synchrotron Radiation Facility, BP 220, F 38043 Grenoble, France

ABSTRACT

Disorder in stoichiometric magnesioferrite, $MgFe_2O_4$, was determined from in situ synchrotron powder X-ray diffraction data [$\lambda = 0.3738(4)$ Å] at 6, 5, and 3 GPa and temperatures up to 1430 K. The *a* unit-cell parameter increases linearly on heating at the three different pressures. Higher pressures cause a smaller cell volume, as expected. Cation order was analyzed in terms of the inversion parameter, *x*, $\{^{iv}[Mg_{1-x}Fe_x]^{vi}[Mg_{x/2}Fe_{1-x/2}]_2O_4\}$ and the order parameter $Q = 1 - (3/2)x$. As pressure increases, the inversion parameter increases in inverse $MgFe_2O_4$ spinel. O'Neill and Navrotsky (1983) and Landau models were used to describe the equilibrium non-convergent ordering process in $MgFe_2O_4$, and they both fit the data well.

INTRODUCTION

Cation order-disorder processes are important in understanding stabilities of minerals in the Earth's mantle. Numerous studies have been carried out on spinels because of their chemical and structural simplicity, their geological importance, and their use as geothermometers, geobarometers, and geospeedometers (e.g., O'Neill and Wall 1987; Sack 1982). Recently, the first in situ high-pressure and high-temperature experimental work on a normal spinel, $MgAl_2O_4$, was carried out (Méducin et al. 2004) and this study investigates cation disorder at high pressures and high temperatures in an inverse magnesioferrite spinel, $MgFe_2O_4$.

Spinels have the general formula AB_2O_4. The structure consists of tetrahedrally coordinated cations at 8*a* (1/8, 1/8, 1/8), octahedrally coordinated cations at 16*d* (1/2, 1/2, 1/2), and O atoms on the body diagonals of a cube at 32*e* (*u*, *u*, *u*), where *u* is approximately 1/4 in space group $Fd\bar{3}m$. In fully "normal" spinels, the A cation occupies the tetrahedral (iv) site and the B cation occupies the octahedral (vi) site, $^{iv}[A]^{vi}[B]_2O_4$. In fully "inverse" spinels, the tetrahedral site contains only B cations and the octahedral site contains an equal number of A and B cations, so the octahedral site is disordered, $^{iv}[B]^{vi}[AB]O_4$. Any intermediate spinel may be expressed as a mix of the normal and inverse endmembers with the general formula: $^{iv}[A_{1-x}B_x]^{vi}[A_{x/2}B_{1-x/2}]_2O_4$, where *x* is denoted the "inversion parameter". This *x* is the fraction of B cations (in this case Fe^{3+}) at the tetrahedral site. In normal spinels, $x = 0$, and in inverse spinels, $x = 1$. A value of $x = 2/3$ corresponds to a completely random distribution of A and B cations. In addition, an order parameter, *Q*, is used to express the degree of order in spinel (see Harrison et al. 1998). The parameter *Q*, varies from $Q = 1$ for a completely ordered normal spinel; to $Q = 0$ (where $x = 2/3$) for a random arrangement of cations; to $Q = -0.5$ in inverse spinel. The relationship between *Q* and *x* is: $Q = 1 - (3/2)x$. The order-disorder process in spinels is termed "non-convergent" because there is no symmetry change upon cation disordering.

Relationships between the cubic cell parameter, *a*, and the inversion parameter, *x*, exist for some spinels. For nearly "normal" spinels, the lattice parameter, *a*, of $ZnAl_2O_4$ (O'Neill and Dollase 1994) increases with the inversion parameter, *x*; for $CoAl_2O_4$ *a* shows no change with *x*, while for $ZnFe_2O_4$ and $MgAl_2O_4$, *a* decrease with *x* (O'Neill, personal communication). For $FeAl_2O_4$, *a* increases very slightly with *x* at low temperature, but then decreases above ~900 ºC, probably due to non-stoichiometry (Larsson et al. 1994). Therefore, no simple generalization is possible between *a* and *x*. Hazen and Yang (1999) predicted that the inverse form of $MgFe_2O_4$ has a larger molar volume and is more compressible than the normal form. Recent in situ high temperature studies of $MgFe_2O_4$ discuss the variation of cation ordering with temperature (Antao et al. 2005; Levy et al. 2004).

In the present in situ study, the pressure effect on cation order has been determined for magnesioferrite at 6, 5, and 3 GPa and temperatures up to 1430 K. These results are used to compare the O'Neill and Navrotsky (1983) thermodynamic model with the Landau (Carpenter et al. 1994; Carpenter and Salje 1994) thermodynamic model for equilibrium cation ordering.

EXPERIMENTAL METHODS

In situ high-pressure and high-temperature synchrotron powder X-ray diffraction

The brown $MgFe_2O_4$ sample was synthesized from equimolar amounts of dried reagent-grade oxides: MgO (slightly excess) and Fe_2O_3. Chemical analysis of the sample shows that it is stoichiometric and additional details are given elsewhere (Antao et al. 2005).

In situ high-temperature and high-pressure synchrotron powder X-ray diffraction experiments were performed at the high-pressure beamline ID30 [$\lambda = 0.3738(4)$

* E-mail sytle.antao@stonybrook.edu

0003-004X/05/0010–1500$05.00/DOI: 10.2138/am.2005.1797

Å] of the European Synchrotron Radiation Facility with the Paris-Edinburgh large-volume apparatus (Besson et al. 1992). The sample was dried in an oven at 423 K for 1 day prior to loading into a gold capsule, which was crimped shut. Room pressure and temperature data were first collected and then the pressure was increased to about 6 GPa and annealed to about 1023 K to eliminate deviatoric stress. The temperature was then lowered to about 650 K and diffraction traces were collected at different temperatures up to 1150 K. Two other cycles at lower pressures were carried out: at 5 GPa up to 1130 K, and at 3 GPa up to 1430 K. To avoid grain growth, the annealing temperature was limited to 1023 K, and the experiments at 6 and 5 GPa were limited to 1150 and 1130 K, respectively. The few data points collected on cooling show a little scatter with respect to the heating data, so they were not included in the thermodynamic models. Pressure and temperature data were obtained by cross-calibration techniques (Crichton and Mezouar 2002), using the equation of state of the capsule materials: gold (Anderson et al. 1989) and hexagonal boron nitride (Le Godec et al. 2000). In the present study, the errors in pressure and temperature are estimated to be about 0.2 GPa and 50 K. Diffraction data were collected with a MarResearch image-plate detector (Mar345) with 100 micrometer resolution after calibration of detector distortion and sample-to-detector distance using NBS660a LaB_6 powder (a = 4.1569 Å) with the Fit2D program (Hammersley et al. 1995). The two-dimensional images were integrated to produce conventional 2θ-I patterns with Fit2D (Hammersley et al. 1996). Use of a multichannel collimator significantly reduced the background contribution from the high-pressure cell assembly (Mezouar et al. 2002). X-ray data were collected to a maximum 2θ of about 27.5° [(sin θ/λ) < 0.64/Å].

Rietveld structure refinements

The diffraction traces were analyzed with the Rietveld method using GSAS and EXPGUI programs (Larson and Von Dreele 2000; Toby 2001). For the room-temperature structure, the starting atomic coordinate, cell parameter, isotropic displacement parameters, and space group, $Fd\bar{3}$m [origin ($\bar{3}m$) at 1/8, 1/8, 1/8 from ($4\bar{3}m$)], were from (O'Neill et al. 1992). Initially, the 8a and 16d cation sites and the 32e O atom sites were constrained to be fully occupied, i.e., the site occupancies were fixed to the idealized stoichiometric chemical formula $MgFe_2O_4$.

The background was modeled using between three and twenty-coefficient Chebyschev polynomial function of the first kind. The reflection profiles were fitted using two coefficients (GW and LY). A full-matrix least-squares refinement varying a scale factor, cell parameter, atomic coordinate, and isotropic displacement parameters converged quickly. The cations at equivalent sites were constrained to have equal isotropic displacement parameters (e.g., Mg^{2+} and Fe^{3+} cations at an 8a site). The cation site occupancy factor, x, which is the fraction of Fe^{3+} cations at the tetrahedral site, was introduced as a variable and refined. Toward the end of the refinement, all parameters (3 to 20 background terms, 2 profile parameters, 1 cell, 1 scale factor, and 5 structural parameters; total variables, P = 12–29) were allowed to vary and the refinement proceeded to convergence. The number of observed reflections in a typical XRD trace is 45, and the number of observations (data points) is about 2000. An example synchrotron X-ray powder-diffraction pattern is shown in Figure 1. The structural parameters and the Rietveld refinement statistics at various temperatures are listed in Table 1.

Results and discussion

The room pressure and temperature structure, based on the data collected at the ESRF, has a = 8.39747(5) Å and inversion parameter x = 0.837(4) and is similar to that obtained by Antao et al. (2005) for the same magnesioferrite sample. The a parameter of $MgFe_2O_4$ increases linearly on heating at 3, 5, and 6 GPa (Table 1; Fig. 2a). Room-pressure data from Antao et al. (2005), which increases linearly, are also included in Figure 2a for comparison. The linear trend lines at room pressure, 5, and 6 GPa are nearly parallel to each other, but the 3 GPa trend line is at an angle to the other trend lines (Fig. 2a). Higher pressure causes a smaller cell volume, as expected (Table 1, Fig. 2a).

Cation order in $MgFe_2O_4$ is displayed in Figure 2b. At 6 GPa and 630 K, x = 0.906(8), which is higher than the initial starting value of 0.837(4) at room pressure and temperature. Therefore, pressure favors a more ordered state in magnesioferrite. Increasing order occurs because the sample was annealed to about 1023 K to eliminate deviatoric stress and this process causes the cations to re-equilibrate. The value of x = 0.906(8) is probably frozen in during the annealing process. The maximum disorder observed at 6 GPa is x = 0.877(5) at 1150 K.

The x value is reduced as the pressure is decreased from 6 to 5 GPa, indicating that cation order is sensitive to pressure, and lower pressure causes more disorder (Fig. 2b). The maximum disorder observed in the experiment at 5 GPa is x = 0.857(7) at 1130 K.

With decreasing pressure to 3 GPa, the cation distribution moves to a more disordered state [x = 0.884(7) at 730 K]. Cation disorder is nearly constant up to about 970 K because of the slow kinetics within this temperature range. From about 1050 K, the cations disorder along a smooth probable equilibrium pathway up to 1430 K. This pathway crosses the curve for the results at room pressure at about 1180 K. The maximum disorder observed at 3 GPa is x = 0.691(7) at 1430 K.

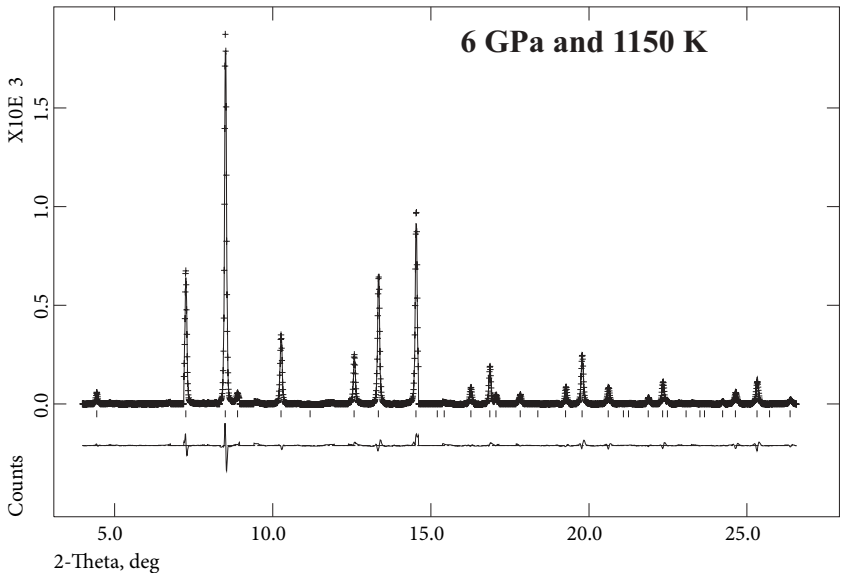

Figure 1. Synchrotron X-ray powder-diffraction pattern for $MgFe_2O_4$ at 6 GPa and 1150 K, together with the calculated (continuous line) and observed (crosses) profiles. The difference curve ($I_{obs} - I_{calc}$) is shown at the bottom. The short vertical lines indicate allowed reflection positions. This pattern is similar to that obtained at room pressure (see Fig. 2 in Antao et al. 2005).

TABLE 1. Magnesioferrite: Rietveld refinement and structural data (top: 6 GPa, middle: 5 GPa, and bottom: 3 GPa)

T (K)	*Time (h)	*a* (Å)	*x*	*u*	R_p	R_{wp}	R_F^2	$U(O) \times 10^2$ (Å^2)	$U(tet) \times 10^2$ (Å^2)	$U(oct) \times 10^2$ (Å^2)	l_{tet-O} (Å)	l_{oct-O} (Å)
Heating												
640	3.12	8.32016(9)	0.906(8)	0.2577(4)	0.0489	0.0645	0.0606	0.39(11)	0.62(8)	0.10(7)	1.912(6)	2.018(3)
740	1.80	8.32711(8)	0.917(7)	0.2578(3)	0.0452	0.0594	0.0783	0.39(9)	0.82(6)	0.20(6)	1.915(5)	2.019(3)
885	0.88	8.33588(8)	0.918(7)	0.2573(4)	0.0447	0.0600	0.0821	0.78(10)	0.99(7)	0.44(6)	1.910(5)	2.025(3)
1020	0.40	8.34613(8)	0.900(6)	0.2570(3)	0.0415	0.0559	0.1085	0.97(9)	1.03(6)	0.73(6)	1.908(5)	2.030(3)
1150	0.50	8.35490(7)	0.877(5)	0.2569(3)	0.0373	0.0501	0.1238	1.10(9)	1.11(6)	0.90(5)	1.909(4)	2.033(2)
Cooling												
970		8.34531(8)	0.891(6)	0.2575(3)	0.0390	0.0513	0.1147	0.84(10)	0.96(7)	0.69(6)	1.915(5)	2.026(3)
860		8.33630(8)	0.918(6)	0.2576(3)	0.0438	0.0603	0.0894	0.66(9)	0.89(6)	0.48(6)	1.914(5)	2.023(3)
700		8.32646(8)	0.920(6)	0.2576(3)	0.0390	0.0513	0.1147	0.45(9)	0.71(6)	0.29(6)	1.912(4)	2.020(2)
Heating												
675	5.50	8.33637(9)	0.907(9)	0.2562(4)	0.0534	0.0724	0.0708	0.62(11)	0.71(7)	0.34(7)	1.894(6)	2.034(3)
770	2.83	8.34432(9)	0.912(8)	0.2569(4)	0.0467	0.0648	0.0889	0.57(10)	0.69(7)	0.34(7)	1.907(6)	2.030(3)
920	0.98	8.35460(9)	0.910(8)	0.2567(4)	0.0474	0.0652	0.0742	0.81(11)	0.88(8)	0.58(7)	1.905(6)	2.035(3)
1070	0.43	8.36537(8)	0.882(7)	0.2561(4)	0.0451	0.0610	0.0910	1.10(10)	1.12(7)	0.80(7)	1.900(6)	2.041(3)
1130	0.45	8.37304(8)	0.857(7)	0.2559(4)	0.0415	0.0561	0.0978	1.47(10)	1.14(7)	0.91(6)	1.898(5)	2.045(3)
Cooling												
1010		8.37303(8)	0.874(6)	0.2565(3)	0.0444	0.0603	0.0775	1.16(10)	1.48(7)	0.74(6)	1.907(5)	2.041(3)
870		8.35489(8)	0.913(6)	0.2564(4)	0.0563	0.0790	0.1326	0.53(10)	1.25(6)	0.20(5)	1.902(5)	2.036(3)
620		8.33319(8)	0.908(7)	0.2574(4)	0.0525	0.0737	0.0858	0.23(9)	0.62(6)	0.01(5)	1.910(5)	2.024(3)
730	2.92	8.36741(8)	0.884(7)	0.2566(4)	0.0511	0.0696	0.0905	0.45(10)	0.49(7)	0.24(6)	1.907(6)	2.038(3)
815	1.93	8.37647(7)	0.883(7)	0.2565(4)	0.0475	0.0650	0.0806	0.59(9)	0.56(6)	0.31(6)	1.907(5)	2.042(3)
960	1.03	8.38915(8)	0.880(8)	0.2559(4)	0.0478	0.0654	0.1062	0.89(10)	0.93(7)	0.61(6)	1.902(6)	2.049(3)
1045	0.85	8.40123(7)	0.844(7)	0.2557(4)	0.0445	0.0611	0.1145	1.26(10)	1.07(7)	0.96(6)	1.902(5)	2.053(3)
1090	0.77	8.41012(8)	0.807(8)	0.2562(4)	0.0443	0.0595	0.0666	1.63(11)	1.19(8)	1.14(7)	1.912(6)	2.052(3)
1110	1.45	8.41455(7)	0.794(7)	0.2558(4)	0.0423	0.0581	0.1077	1.58(10)	1.06(7)	1.10(6)	1.906(5)	2.056(3)
1220	0.07	8.42331(7)	0.764(6)	0.2552(4)	0.0408	0.0567	0.1825	1.63(10)	0.94(7)	1.33(6)	1.899(5)	2.063(3)
1310	0.08	8.43440(7)	0.742(7)	0.2555(4)	0.0444	0.0632	0.2597	2.15(12)	0.99(8)	1.62(7)	1.906(6)	2.064(3)
1430	0.07	8.44786(7)	0.691(7)	0.2551(4)	0.0429	0.0615	0.2029	2.72(12)	1.15(8)	1.88(7)	1.904(5)	2.070(3)
Cooling												
1320		8.44044(9)	0.687(9)	0.2555(6)	0.0589	0.0833	0.2189	3.17(17)	1.17(9)	1.63(9)	1.908(8)	2.065(4)
1210		8.43331(9)	0.744(9)	0.2554(5)	0.0769	0.1056	0.2017	4.23(18)	1.63(9)	1.55(9)	1.904(8)	2.064(4)
1130		8.42484(8)	0.741(7)	0.2566(4)	0.0535	0.0801	0.1279	2.91(14)	0.64(8)	1.37(7)	1.921(6)	2.052(4)
1070		8.41798(8)	0.777(7)	0.2573(4)	0.0540	0.0796	0.1231	2.07(13)	0.57(7)	1.04(7)	1.929(6)	2.045(3)
1030		8.41033(8)	0.798(7)	0.2576(4)	0.0549	0.0814	0.1244	0.95(12)	0.38(7)	0.72(7)	1.932(6)	2.040(3)
890		8.39887(9)	0.809(8)	0.2565(5)	0.0666	0.0964	0.1419	0.90(13)	0.23(8)	0.64(7)	1.912(7)	2.047(4)
560		8.38636(9)	0.814(9)	0.2564(5)	0.0755	0.1097	0.1521	0.60(14)	0.23(8)	0.41(8)	1.909(7)	2.044(4)

Notes: R_p = pattern *R* factor = $\{\sum(|I_o - I_c|)\}/\sum I_o$; R_{wp} = weighted pattern *R* factor = $\{\sum[w(I_o - I_c)^2]/\sum[wI^2_o]\}^{1/2}$, where I_o = observed intensity, I_c = calculated intensity, and $w = 1/I_o$; R_p and R_{wp} are the fitted values obtained without background subtraction. R_F^2 = *R*-structure factor based on observed and calculated structure amplitudes = $\{\sum(|F_o^{1/2} - F_c^{1/2}|)\}/\sum F_o^{1/2}$.

* The time given in hours represents the amount of time the sample was kept at that particular temperature to achieve equilibrium before data collection. Cooling data were collected without any time for re-equilibration, so no time information is given.

An activation barrier (relaxation toward equilibrium) was observed at room pressure where data were collected continuously with increasing temperature (see Fig. 4 in Antao et al. 2004). The activation barrier in the room-pressure data set is seen as a "hump" at about 850 K in Figure 2b. With the annealing process at 6 GPa, the activation barrier is overcome, and is not observed in the high-pressure data sets. Therefore, at 6, 5 and 3 GPa, the cation distribution remains nearly constant initially at low temperatures, and then follows the equilibrium curve (Fig. 2b). The region where *x* is about constant is indicated by horizontal lines in Figures 2b and 2c.

As pressure increases, the inversion parameter, *x*, increases in inverse $MgFe_2O_4$ spinel (the sample becomes more ordered). This can be seen if a vertical line is drawn at about 1050 K in Figure 2b. The 3 GPa data appear to be anomalous, because at low temperature the data are more ordered than at room pressure, but at higher temperature (about 1100 K) the 3 GPa data are more disordered than the room pressure data (Fig. 2b).

Recent studies have shown that with increasing pressure, the inversion parameter increases in both inverse $NiAl_2O_4$ spinel (Halevy et al. 2002) and normal $MgAl_2O_4$ spinel (Méducin et al. 2004). Therefore, pressure acts against temperature in inverse $MgFe_2O_4$ and $NiAl_2O_4$ spinels, and with temperature in normal $MgAl_2O_4$ spinel. Volume of disordering, ΔV_{dis} (= $V_{dis} - V_{ord}$), appears to be an important factor in predicting the effect of pressure on the inversion parameter. Using the geometrical formula for the unit cell, ΔV_{dis} can be calculated using appropriate radii (Hazen and Navrotsky 1996). This calculation shows that ΔV_{dis} is negative for normal spinel $MgAl_2O_4$, and positive for the inverse spinels $MgFe_2O_4$ and $NiAl_2O_4$. Therefore, with a negative ΔV_{dis} (as in $MgAl_2O_4$), increasing pressure would favor the disordered state as that has a smaller volume compared to the ordered state. Whereas, in $MgFe_2O_4$ and $NiAl_2O_4$, pressure favors a more ordered state as ΔV_{dis} is positive (i.e., the ordered state has the smaller volume).

Figure 2c shows the variation of *x* with the *a* cell parameter. The first two data points at lower temperatures for the three different pressures are probably at non-equilibrium, and at higher temperatures, the *x* values occur along the three different equilibrium pathways. These equilibrium pathways are nearly parallel to each other and also parallel to that observed at room pressure. If the curves are extrapolated to the *a* cell-parameter axis, it can be seen that high pressure gives rise to a smaller unit cell for the same value of disorder (e.g., for a completely disordered state

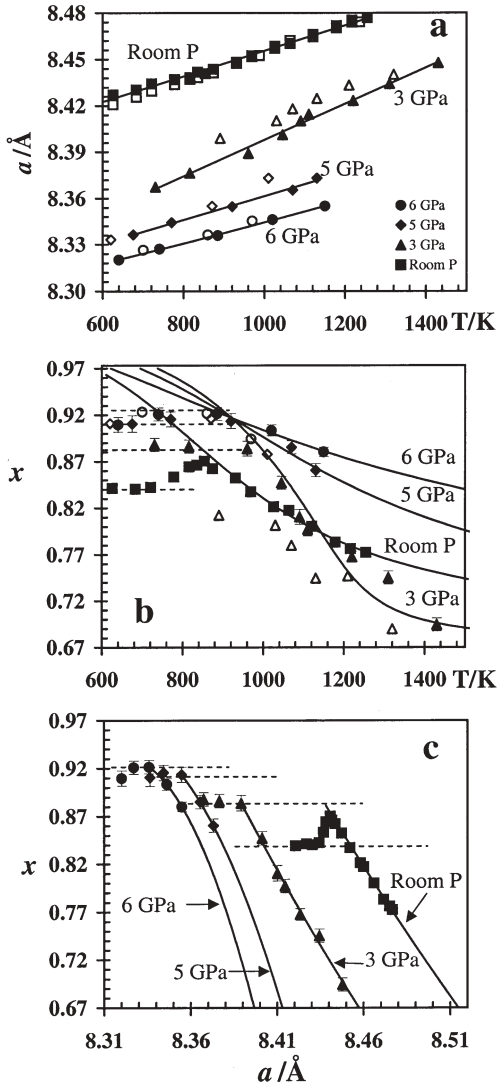

FIGURE 2. Structural variations at 6, 5, and 3 GPa for $MgFe_2O_4$ on heating (solid symbols) and on cooling (open symbols). (**a**) The *a* unit-cell parameter vs. temperature. (**b**) Inversion parameter, *x* vs. temperature. Solid curves are the O'Neill and Navtrosky (1983) models applied to our equilibrium data. (**c**) *x* vs. *a*. Error bars are not seen if smaller than the symbols. Room pressure data from Antao et al. (2005) are included for comparison to this and other figures below. The region where *x* is about constant is indicated by horizontal lines in Figures 2b and 2c.

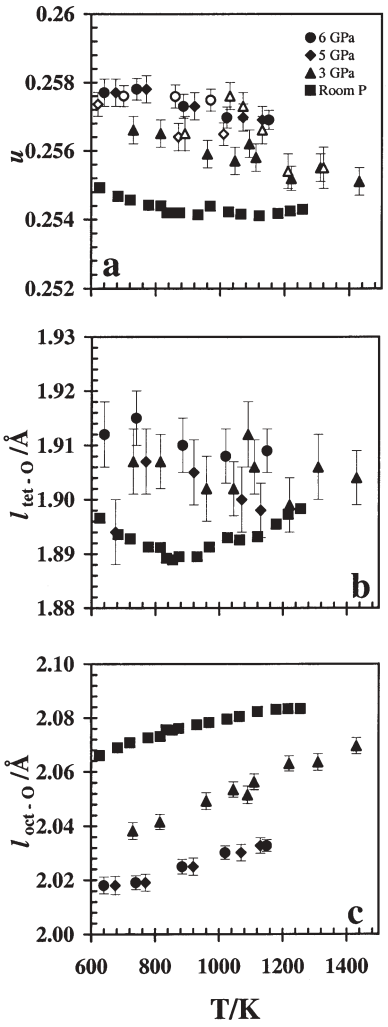

FIGURE 3. Variations in structural parameters for $MgFe_2O_4$ at 6, 5, and 3 GPa: (**a**) *u* vs. temperature on heating (solid symbols) and on cooling (open symbols), (**b**) l_{tet-O} vs. temperature, and (**c**) l_{oct-O} vs. temperature.

where $x = 0.67$: $a \approx 8.387$ Å at 6 GPa; $a \approx 8.413$ Å at 5 GPa; $a \approx 8.457$ Å at 3 GPa; and $a \approx 8.514$ Å at room pressure; Fig. 2c). The effect of pressure on the relationship between the cell parameter and the inversion parameter is quite large for $MgFe_2O_4$.

The oxygen positional parameter, *u*, decreases gradually with increasing temperature (Fig. 3a). The *u* values at 5 and 6 GPa are similar to each other, while that at 3 GPa is offset to lower values. The *u* parameter is also sensitive to the state of cation order. The *x* values observed at 5 and 6 GPa are similar and therefore the *u* values are also similar (Figs. 2b and 3a).

Figures 3b and 3c display the variation of the tetrahedral cation to O atom bond distance (l_{tet-O}) and the octahedral cation to O atom (l_{oct-O}) bond distance. The octahedral site affects the cell parameter more than the tetrahedral site because the l_{tet-O} distance is nearly constant. Similar effects were observed at room pressure (Antao et al. 2005). The l_{tet-O} distance at the three different pressures are similar within experimental error (Fig. 3b). All the l_{oct-O} distances increase linearly with temperature. The l_{oct-O} distance at 3 GPa is higher than at 5 or 6 GPa (Fig. 3c).

THERMODYNAMIC MODELING

Details on modeling the cation distribution in magnesioferrite were recently described (Antao et al. 2005), so only a brief description is given here. The O'Neill and Navrotsky (1983) model relates the enthalpy per formula unit of a spinel with an intermediate cation distribution, relative to the same spinel with a normal cation distribution, as a function of *x*. The equilibrium pathway for *x* is given by the following expression relating *x* and *T*:

$$-RT \ln \{(x^2/(1-x)(2-x)\} = \alpha + 2\beta x \quad (1)$$

This model provides a good fit to our experimental data (solid curve; Fig. 4). A multiple non-linear least-squares fit to our equilibrium data (excluding the first two lowest-temperature data points at the three different pressures) yields: $\alpha = -10.7$ kJ/mol and $\beta = -33.0$ kJ/mol ($R^2 = 0.9933$) at 6 GPa, $\alpha = +23.2$ kJ/mol and $\beta = -21.9$ kJ/mol ($R^2 = 0.9754$) at 5 GPa, and $\alpha = +43.7$ kJ/mol and $\beta = -33.1$ kJ/mol ($R^2 = 0.9599$) at 3 GPa. At room pressure, $\alpha = +24.8$ kJ/mol and $\beta = -21.1$ kJ/mol ($R^2 = 0.9907$; Antao et al. 2005). With our limited data, particularly at high temperatures, we are presently unable to rationalize these α and β values. Moreover, with uncertainties as large as 50 K and 0.2 GPa in our data, these α and β values may not be reliable.

In the Landau model, the free energy of an intermediate spinel is calculated relative to a hypothetical spinel with a fully disordered cation distribution. The order parameter, Q, is chosen such that complete disorder corresponds to $Q = 0$ where $Q = 1 - (3/2)x$. Applying the constraint that $Q = -0.5$ at 0 K for inverse spinel results in the equilibrium condition:

$$T = T_c + [0.5T_c\,(1-c'Q^5)]/(c'0.5^5 + 1)Q,$$

where $c' = c/h$ (Harrison and Putnis 1997).

A least-squares fit to our equilibrium data yields the following results: at 6 GPa, $T_c = 933$ K and $c' = -148$ ($R^2 = 0.9991$); at 5 GPa, $T_c = 1407$ K and $c' = 567$ ($R^2 = 0.9968$); and at 3 GPa, $T_c = 1113$ K and $c' = -1494$ ($R^2 = 0.9540$). At room pressure, $T_c = 705$ K and $c' = -165$ ($R^2 = 0.9919$; (Antao et al. 2005). The result of the fit is shown as the dashed curve in Figure 4. At 5 and 6 GPa, only 3 data points were used and therefore, the fits may not be reliable. The c' for data at 5 GPa is the only one that has a positive value, so the Landau model for the 5 GPa data set curves back in the opposite direction beyond about 1190 K (Fig. 4). Again, because of our limited data we cannot presently rationalize the Landau coefficients. In general, O'Neill and Navrotsky (1983) and Landau thermodynamic models describe the equilibrium ordering process fairly well for $MgFe_2O_4$ within the range where experimental data is obtained. Nevertheless, the two models for the data sets at room pressure and 3 GPa match quite well except at low temperatures. However, both models for the 5 and 6 GPa data sets do not match each other outside the present data range, which could result from the fact that only three data points were available.

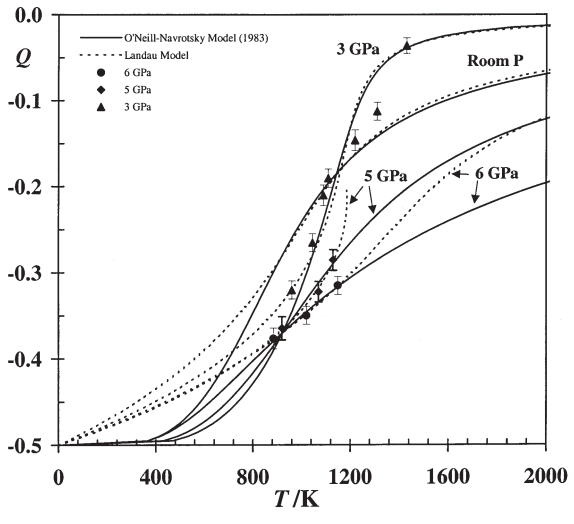

FIGURE 4. Thermodynamic models: solid curve is the fit to our data using O'Neill and Navrotsky (1983) model. Dashed curve is the fit to our data using the Landau model. At 5 and 6 GPa, only three data points were used, so the fits may be unreliable.

The room-temperature lattice parameter data from O'Neill et al. (1992) for samples of $MgFe_2O_4$ quenched from different temperatures between 450 and 1150 ºC gave the volume and inversion parameter relationship as (see Eq. 7 in O'Neill et al. 1992):

$$V\,(\text{cm}^3/\text{mol}) = 45.80 - 1.65x.$$

The volume of disordering, $\Delta V_{dis} = V_{disorder} - V_{order} = 44.70$ (where $x = 2/3$) $- 44.15$ (where $x = 1$) $= 0.55$ cm^3/mol. When bond distances are used to calculate ΔV_{dis} for magnesioferrite, a positive value is also obtained, as mentioned previously.

The ΔV_{dis} can be obtained by fitting our equilibrium data to the following expression and using a global regression fit:

$$-RT \ln \{(x^2/(1-x)(2-x)\} = \alpha + 2\beta x + \Delta V_{dis}{}^*P \qquad (2).$$

This equation is the same as Equation. 1, but with an extra term for the pressure variable. Using only equilibrium data, we used the three data points from the 60 kbar cycle above 885 K. For the 1 bar data, the lowest temperature equilibrium data is assumed to be 658 ºC (Antao et al. 2005). With these data, curve fitting produced the following global values: $\alpha = +26.0$ kJ/mol, $\beta = -21.9$ kJ/mol, and $\Delta V_{dis} = -58.5$ J/(kbar-mol). Including the 50 and 30 kbar data does not significantly affect these values. Using these values and the different pressures, the resulting curve at

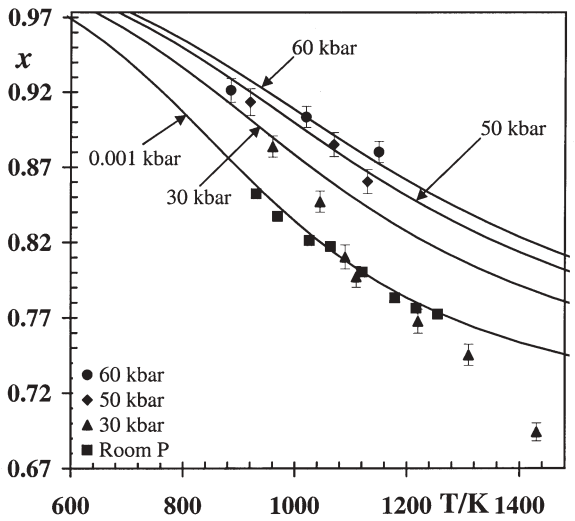

FIGURE 5. Fit to our equilibrium data using O'Neill and Navrotsky (1983) model and including a volume of disordering term: $-RT \ln \{(x^2/(1-x)(2-x)\} = \alpha + 2\beta x + \Delta V_{dis}{}^*P$. Using the following global values: $\alpha = +26.0$ kJ/mol, $\beta = -21.9$ kJ/mol, and $\Delta V_{dis} = -58.5$ J/(kbar-mol) and the appropriate pressure (in kbar) in the above equation, the solid curves are produced and they match the experimental data points quite well, except for the 30 kbar data points, which appear unreliable.

a particular pressure matches the experimental data at the same pressure quite well, except for the 30 kbar data (Fig. 5). In addition, the value of ΔV_{dis} [= –58.5 (J/kbar-mol)] obtained by this method is about three times smaller than the expected value [= –165 (J/kbar-mol)]. This disagreement and the poor fit for the 30 kbar data indicate that something may have happened in the sample, for example, some degree of reduction might have occurred at 3 GPa, so this effect requires further investigation.

ACKNOWLEDGMENTS

D.H. Lindsley is thanked for his help in synthesizing and chemically analyzing the magnesioferrite sample. C.D. Martin is thanked for his help with data collection. J. Chen is thanked for useful discussions. We thank the reviewers, S.A.T. Redfern, H.St.C. O'Neill, and A. Pawley for useful comments. In particular, we thank O'Neill for discussion of the volume of disorder and the global regression fit. This study was supported by NSF grant EAR-0125094 and EAR-0510501 to J.B.P. The experimental work was performed at ID30 of the ESRF, no. HS2130.

REFERENCES CITED

Anderson, O.L., Isaak, D.G., and Yamamoto, S. (1989) Anharmonicity and the equation of state for gold. Journal of Applied Physics, 65, 1534–1543.

Antao, S.M., Hassan, I., and Parise, J.B. (2005) Cation ordering in magnesioferrite, $MgFe_2O_4$, to 982 °C using in situ synchrotron X-ray powder diffraction. American Mineralogist, 90, 219–228.

Besson, J.M., Nelmes, R.J., Hamel, G., Loveday, J.S., Weill, G., and Hull, S. (1992) Neutron powder diffraction above 10-GPa. Physica B, 180, 907–910.

Carpenter, M.A. and Salje, E.K.H. (1994) Thermodynamics of nonconvergent cation ordering in minerals: II. Spinels and the ortho-pyroxene solid-solution. American Mineralogist, 79, 1068–1083.

Carpenter, M.A., Powell, R., and Salje, E.K.H. (1994) Thermodynamics of nonconvergent cation ordering in minerals: I. An alternative approach. American Mineralogist, 79, 1053–1067.

Crichton, W.A. and Mezouar, M. (2002) Noninvasive pressure and temperature estimation in large-volume apparatus by equation-of-state cross-calibration. High Temperatures-High Pressures, 34, 235–242.

Halevy, I., Dragoi, D., Ustundag, E., Yue, A.F., Arredondo, E.H., Hu, J.Z., and Somayazulu, M.S. (2002) The effect of pressure on the structure of $NiAl_2O_4$. Journal of Physics-Condensed Matter, 14, 10511–10516.

Hammersley, A.P., Svensson, S.O., Thompson, A., Graafsma, H., Kvick, A., and Moy, J.P. (1995) Calibration and correction of distortions in 2-dimensional detector systems. Review of Scientific Instruments, 66, 2729–2733.

Hammersley, A.P., Svensson, S.O., Hanfland, M., Fitch, A.N., and Hausermann, D. (1996) Two-dimensional detector software: from real detector to idealised image or two-theta scan. High Pressure Research, 14, 235–248.

Harrison, R.J. and Putnis, A. (1997) The coupling between magnetic and cation ordering: A macroscopic approach. European Journal of Mineralogy, 9, 1115–1130.

Harrison, R.J., Redfern, S.A.T., and O'Neill, H.S.C. (1998) The temperature dependence of the cation distribution in synthetic hercynite ($FeAl_2O_4$) from in-situ neutron structure refinements. American Mineralogist, 83, 1092–1099.

Hazen, R.M. and Navrotsky, A. (1996) Effects of pressure on order-disorder reactions. American Mineralogist, 81, 1021–1035.

Hazen, R.M. and Yang, H.X. (1999) Effects of cation substitution and order-disorder on P-V-T equations of state of cubic spinels. American Mineralogist, 84, 1956–1960.

Larson, A.C. and Von Dreele, R.B. (2000) General Structure Analysis System (GSAS). Los Alamos National Laboratory Report, LAUR 86–748.

Larsson, L., O'Neill, H.S.C., and Annersten, H. (1994) Crystal-chemistry of synthetic hercynite ($FeAl_2O_4$) from XRD structural refinements and Mossbauer-spectroscopy. European Journal of Mineralogy, 6, 39–51.

Le Godec, Y., Martinez-Garcia, D., Mezouar, M., Syfosse, G., Itie, J.P., and Besson, J.M. (2000) Equation of state and order parameter in graphite-like h-BN under high pressure and temperature. In M.H. Manghnani, W.J. Nellis, and M.F. Nicol, Eds., Proceedings of AIRAPT-17: Science and Technology of High Pressure, p. 925–928. Universities Press, Hyderabad, India.

Levy, D., Diella, V., Dapiaggi, M., Sani, A., Gemmi, M., and Pavese, A. (2004) Equation of state, structural behaviour and phase diagram of synthetic $MgFe_2O_4$, as a function of pressure and temperature. Physics and Chemistry of Minerals, 31, 122–129.

Méducin, F., Redfern, S.A.T., Le Godec, Y., Stone, H., Tucker, M.G., Dove, M.T., and Marshall, W.G. (2004) Study of cation order-disorder in $MgAl_2O_4$ spinel by in situ neutron diffraction up to 1600 K and 3.2 GPa. American Mineralogist, 89, 981–986.

Mezouar, M., Faure, P., Crichton, W., Rambert, N., Sitaud, B., Bauchau, S., and Blattmann, G. (2002) Multichannel collimator for structural investigation of liquids and amorphous materials at high pressures and temperatures. Review of Scientific Instruments, 73, 3570–3574.

O'Neill, H.S.C. and Dollase, W.A. (1994) Crystal-structures and cation distributions in simple spinels from powder XRD structural refinements—$MgCr_2O_4$, $ZnCr_2O_4$, Fe_3O_4 and the temperature-dependence of the cation distribution in $ZnAl_2O_4$. Physics and Chemistry of Minerals, 20, 541–555.

O'Neill, H.S.C. and Navrotsky, A. (1983) Simple spinels—crystallographic parameters, cation radii, lattice energies, and cation distribution. American Mineralogist, 68, 181–194.

O'Neill, H.S.C. and Wall, V.J. (1987) The olivine ortho-pyroxene spinel oxygen geobarometer, the nickel precipitation curve, and the oxygen fugacity of the Earth's upper mantle. Journal of Petrology, 28, 1169–1191.

O'Neill, H.S.C., Annersten, H., and Virgo, D. (1992) The temperature-dependence of the cation distribution in magnesioferrite ($MgFe_2O_4$) from powder XRD structural refinements and Mossbauer-spectroscopy. American Mineralogist, 77, 725–740.

Sack, R.O. (1982) Spinels as petrogenetic indicators—activity-composition relations at low-pressures. Contributions to Mineralogy and Petrology, 79, 169–186.

Toby, B.R. (2001) EXPGUI, a graphical user interface for GSAS. Journal of Applied Crystallography, 34, 210–221.

MANUSCRIPT RECEIVED AUGUST 28, 2004
MANUSCRIPT ACCEPTED FEBRUARY 11, 2005
MANUSCRIPT HANDLED BY ALISON PAWLEY